I&EC research
Industrial & Engineering Chemistry Research

pubs.acs.org/IECR

Article

Thiourea Modification Promoting the Activity on Pt/CeO_2 for CO Oxidation by Weakening the Metal−Support Interaction

Lijun Ni, Wei Tan,* Bifeng Zhang, Qi Zhang, Jing Xu, Ying Zhang, Chengsi Pan, Yongfa Zhu, Fudong Liu, and Yang Lou*

Cite This: *Ind. Eng. Chem. Res.* 2025, 64, 4835−4844

Read Online

ACCESS | Metrics & More | Article Recommendations | Supporting Information

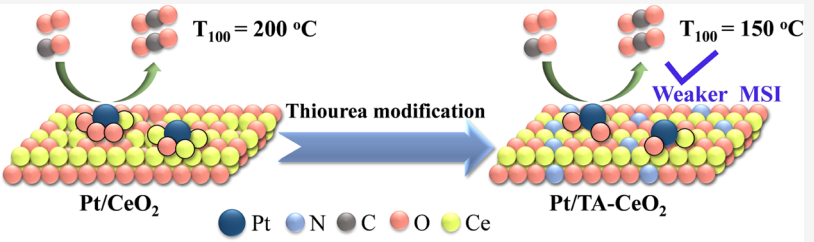

ABSTRACT: Supported metal catalysts play a vital role in the chemical industry; however, ensuring high activity while maintaining high stability remains a significant challenge. Herein, a strategy for modulating the metal−support interactions (MSIs) in CeO_2-supported Pt-based catalyst via doping N into ceria using thiourea as a dopant ($Pt/TA\text{-}CeO_2$) is proposed, through which excellent low-temperature CO oxidation activity and recycling stability are achieved simultaneously. Experimental characterization results demonstrate that the introduction of thiourea properly alters the structural defects and electronic state of Pt in the $Pt/TA\text{-}CeO_2$ catalyst, thereby weakening the metal−support interaction. As a result, the complete conversion temperature of $Pt/TA\text{-}CeO_2$ decreases from 200 to 150 °C while still maintaining high activity after 11 cycles of CO oxidation. This work offers valuable insights into modulating the catalytic capability in essential reactions by regulating the metal−support interactions in supported metal catalysts.

1. INTRODUCTION

Supported metal catalysts are a subset of heterogeneous catalysts that play a crucial role in the chemical industry.[1−6] Noble metals (Pt, Pd, Rh, Au, etc.) supported on oxides (ceria, alumina, titania, etc.) serve as typical CO oxidation catalysts, and the properties of the supports and noble metals significantly affect their catalytic activity and stability.[7−9] Among them, ceria has been commonly utilized as a support for noble metals in the CO oxidation field due to its excellent redox properties and oxygen storage capacity (OSC) via the reversible redox cycle of Ce^{4+}/Ce^{3+} species.[3,10]

It is highly desirable that CO oxidation proceeds at low temperatures while accounting for high stability, low cost, and environmental friendliness.[3] Most of the noble metal nanoparticle-based catalysts are impractical for use under operational conditions due to their low atom efficiency and high cost. Single-atom catalysts (SACs) offer the potential for application under real conditions and significantly decrease the cost of catalysts, which is attributed to the 100% atom efficiency and excellent performance across various catalytic reactions.[11,12] Nevertheless, SACs still have a certain gap in catalytic activity and stability compared to noble metal−supported nanoparticle catalysts due to the limited maximum loadings of SACs and the tendency of agglomeration. Consequently, in the past few years, substantial efforts have been devoted to developing high-performance SACs, including strategies such as modulating the coordination environment (or metal−support interactions (MSIs)),[3,13−15] support modification,[16,17] altering the crystal facet,[8,18] additional coating layer,[19,20] and doping with heteroatoms.[21,22] However, most catalysts currently struggle to simultaneously achieve high CO activity and stability, especially under harsh conditions. Therefore, there is an urgent need to develop new strategies to construct SACs that exhibit excellent low-temperature activity and satisfactory stability.

In terms of oxide-supported noble metal catalysts, metal−support interactions (MSIs) are often reported to be beneficial for catalytic reactions.[3,23] However, Tan et al. recently proposed that the strong metal−support interaction in CeO_2-supported single Pt atoms is detrimental to CO oxidation but beneficial for NH_3 oxidation.[14] Inspired by these findings, we

Received: December 18, 2024
Revised: January 18, 2025
Accepted: February 17, 2025
Published: February 22, 2025

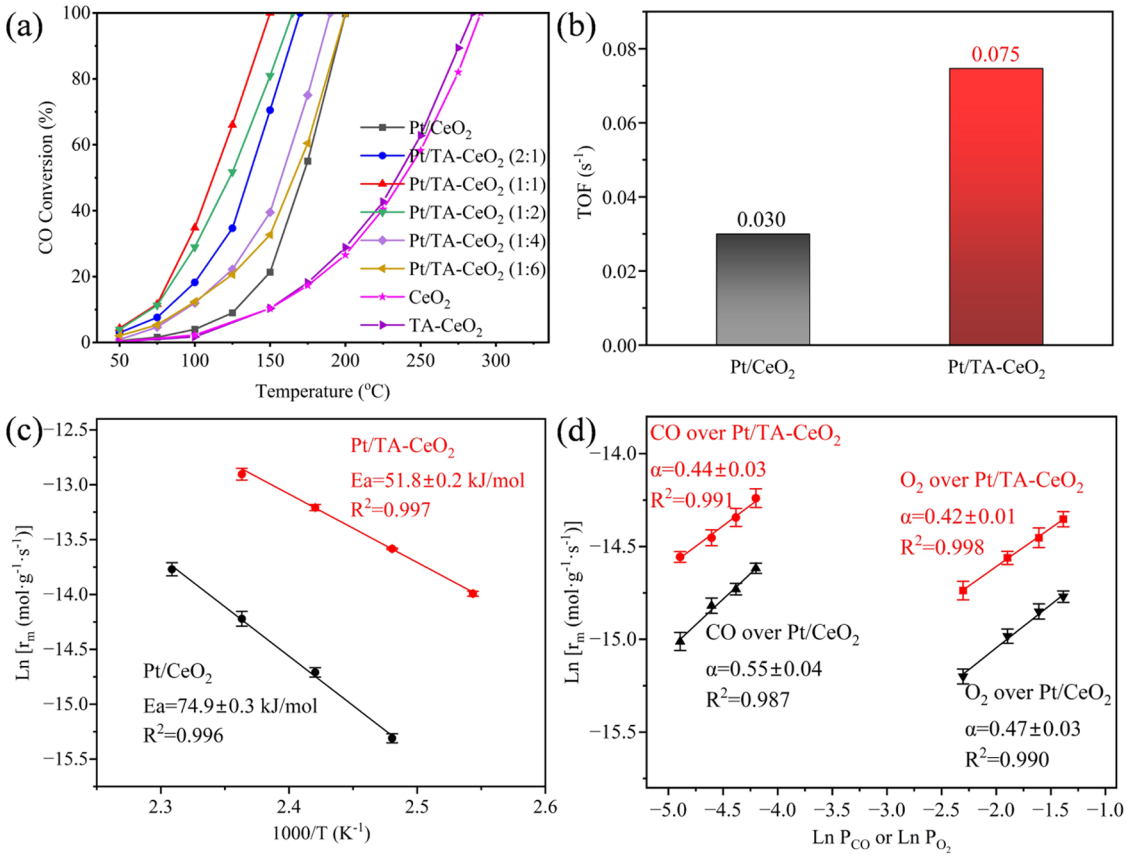

Figure 1. Catalytic performance and reaction kinetics of CO oxidation. (a) CO oxidation activity on CeO_2, TA-CeO_2, Pt/CeO_2, and Pt/TA-CeO_2 with different doping contents of thiourea (reaction conditions: 1 vol % CO and 20 vol % O_2, balanced with Ar, weight hourly space velocity (WHSV) = 25,000 mL·g_{cat}^{-1}·h^{-1}). (b) Comparison of turnover frequency (TOF) for Pt/CeO_2 and Pt/TA-CeO_2 catalysts at 150 °C. (c) Arrhenius plots over Pt/CeO_2 and Pt/TA-CeO_2 catalysts (reaction conditions: 1 vol % CO and 20 vol % O_2, balanced with Ar, WHSV = 150,000 mL·g_{cat}^{-1}·h^{-1}). (d) CO and O_2 reaction orders of Pt/CeO_2 and Pt/TA-CeO_2 catalysts in the CO oxidation reaction.

propose that the catalytic capability of supported metal catalysts can be improved by directionally weakening the MSIs.

In this work, Pt SACs supported on N-doped ceria (Pt/TA-CeO_2) were developed, where thiourea (TA) was introduced into ceria as a dopant via hydrothermal synthesis to weaken the MSI. As a result, Pt/TA-CeO_2 exhibited superior catalytic performance and recycling stability in CO oxidation compared to the reference Pt/CeO_2 samples. Furthermore, the structural characteristics, properties, and MSIs of the synthesized catalysts were thoroughly characterized by Raman spectroscopy, X-ray diffraction (XRD), TEM, EDS, H_2-TPR, UV−vis spectroscopy, *in situ* CO-DRIFTS, and XPS to better understand the experimental results.

2. EXPERIMENTAL SECTION

2.1. Preparation of CeO_2 and TA-CeO_2. All reagents were of analytical grade and were utilized without further purification during the synthesis. In a typical preparation of CeO_2 sample via hydrothermal synthesis,[24] 25 mL of cerium nitrate ($Ce(NO_3)_3·6H_2O$) solution (0.08 M) was slowly added to 25 mL of Na_2CO_3 aqueous solution (0.15 M) under continuous stirring. The mixed solution was stirred for 60 min, and then the obtained solution was transferred to a 100 mL stainless steel autoclave with an inside Teflon liner, which was further heated at 200 °C for 24 h. After the autoclave was cooled to room temperature, the precipitate was separated by centrifugation, washed several times with distilled water and ethanol, and dried at 120 °C for 1 h. Finally, the obtained solid was calcined at 700 °C in nitrogen for 2 h to obtain yellow ceria, denoted as CeO_2. For the TA-CeO_2 (m:n) supports (m:n represents the molar ratio of $Ce(NO_3)_3·6H_2O$ and TA), the only difference in the preparation procedure was that a certain amount of thiourea (TA) was added to the mixed solution of $Ce(NO_3)_3·6H_2O$ and Na_2CO_3.

2.2. Preparation of Pt/CeO_2 and Pt/TA-CeO_2. Pt/CeO_2 and Pt/TA-CeO_2 (m:n) catalysts were prepared by the electrostatic adsorption method. First, CeO_2 or TA-CeO_2 (m:n) was dispersed in an aqueous solution, and the pH was slowly adjusted to 3.0−3.2 by adding HCl dropwise. The corresponding amount of $H_2PtCl_6·6H_2O$ was dissolved in distilled water and added dropwise to the mixture solution under vigorous stirring. After further stirring for 3 h at room temperature, the solution was filtered, washed several times with distilled water and ethanol, and then dried at 120 °C for 1 h. Finally, the dried catalysts were calcined at 700 °C for 2 h under a nitrogen atmosphere.

2.3. Preparation of Urea (UA)-CeO_2 Support and Pt/UA-CeO_2. The other preparation procedure of the UA-CeO_2 support was the same as that of CeO_2. The only difference was that urea (UA) with a molar ratio of 1:1 to $Ce(NO_3)_3·6H_2O$ was added to the mixed solution of $Ce(NO_3)_3·6H_2O$ and Na_2CO_3. Then, the Pt/UA-CeO_2 catalyst was prepared using an electrostatic adsorption method, as shown in Section 2.2.

https://doi.org/10.1021/acs.iecr.4c04820
Ind. Eng. Chem. Res. 2025, 64, 4835−4844

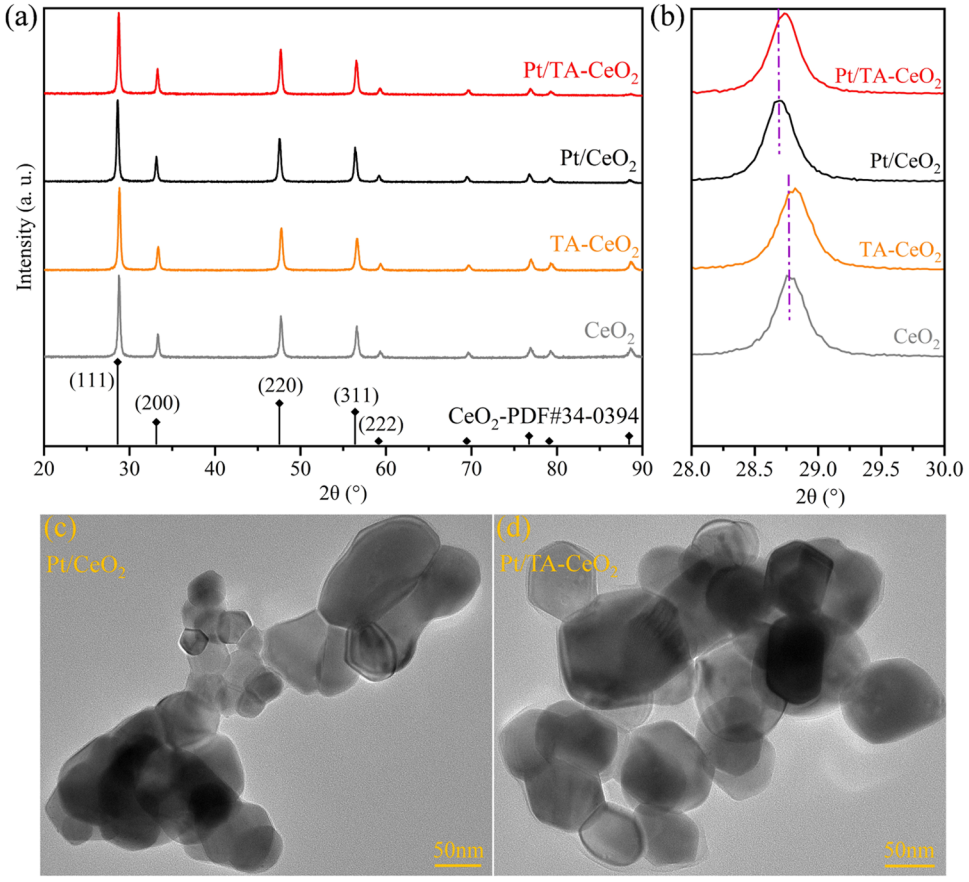

Figure 2. Characterization of thiourea modification. (a) XRD patterns of CeO_2, TA-CeO_2, Pt/CeO_2, and Pt/TA-CeO_2. (b) Shift of the XRD peaks related to the CeO_2 (111) crystal plane. TEM images of (c) Pt/CeO_2 and (d) Pt/TA-CeO_2.

2.4. Catalytic Performance Evaluation and Characterization. The catalytic performance was evaluated in a fixed-bed reactor. Thirty milligrams of the catalyst (40−60 mesh) were mixed with 400 mg of silica. The reaction feeding gas consisted of 1.0% CO, 20.0% O_2, and balanced Ar with a total flow rate of 12.5 mL·min^{-1}, thus giving a weight hourly space velocity (WHSV) of 25,000 mL·g_{cat}^{-1}·h^{-1}. The concentrations of CO and CO_2 in the inlet and outlet streams were detected online using a gas chromatograph equipped with FID detector.

The details of the calculation and characterization are provided in the Supporting Information (Texts S1 and S2).

3. RESULTS AND DISCUSSION

3.1. Catalytic Activity and Reaction Kinetics in the CO Oxidation Reaction. First, the activity of the synthesized Pt catalysts for CO oxidation was evaluated. As presented in Figure 1a, TA modification could significantly improve the CO oxidation activity on Pt/CeO_2, and the CO oxidation activity on Pt/TA-CeO_2 (m:n) followed a volcano trend with increasing molar ratio of Ce to TA. Pt/TA-CeO_2 (1:1) was found to perform the best (Figure S1), with much lower T_{100} and T_{50} (T_{100} of 150 °C and T_{50} of 112 °C; T_{100} or T_{50} is the temperature at which CO conversion reached 100% or 50%) than that of Pt/CeO_2 (T_{100} of 200 °C and T_{50} of 164 °C). For convenience, Pt/TA-CeO_2 (1:1), with the best catalytic performance, was chosen as the representative catalyst for further investigation and labeled Pt/TA-CeO_2 in the following. Comparing the CO oxidation conversion rate of the Pt/CeO_2-based catalyst with recent literature (Table S1), it was found that Pt/TA-CeO_2 developed in this work performed one of the best among the novel catalysts. The comparable CO oxidation activity on TA/CeO_2 (T_{100} of 285 °C and T_{50} of 234 °C) and CeO_2 (T_{100} of 290 °C and T_{50} of 238 °C) suggested that the improved CO oxidation activity on Pt/TA-CeO_2 is associated with the modulated Pt dispersion, Pt-CeO_2, or Pt-TA interaction, rather than the contribution from TA itself. In order to compare the influence of different dopants, Pt/UA-CeO_2 was prepared with urea of the same molar ratio instead of thiourea as the dopant for the CO oxidation activity test, as shown in Figure S2, which shows that the CO oxidation activity of Pt/UA-CeO_2 was comparable with that of Pt/CeO_2, indicating that urea modification could not significantly improve the CO oxidation activity of Pt/CeO_2.

As an important performance indicator, the stability of Pt/TA-CeO_2 was also evaluated using recycling and long-term CO oxidation tests. Unlike Pt/CeO_2, which suffered from severe deactivation in the recycling test (Figure S3a), no obvious decrease in the activity was observed for CO oxidation on Pt/TA-CeO_2 (Figure S3b), highlighting its superior stability under reaction conditions. Meanwhile, after the long-term CO oxidation test of 6 h at T_{90} (Figure S4), although both Pt/CeO_2 and Pt/TA-CeO_2 suffered from deactivation, the decrease in the CO oxidation activity on Pt/TA-CeO_2 (25%) was much less than that on Pt/CeO_2 (43%), further indicating the better stability of Pt/TA-CeO_2.

To gain deep insight into the intrinsic catalytic behaviors of the Pt/CeO_2 and Pt/TA-CeO_2 samples, reaction kinetic data were collected. As shown in Figure 1b, the turnover frequency

https://doi.org/10.1021/acs.iecr.4c04820
Ind. Eng. Chem. Res. 2025, 64, 4835−4844

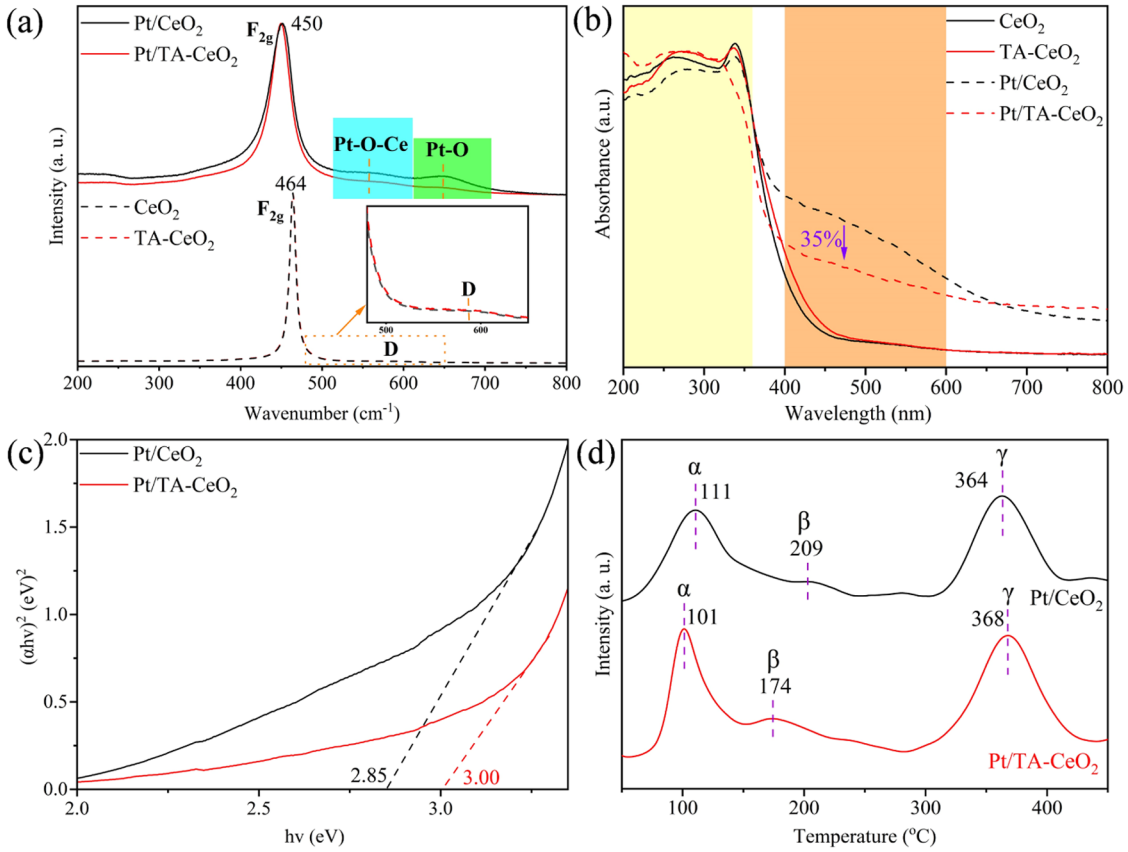

Figure 3. Structural characterization of the metal−support interaction. (a) Raman spectra and (b) UV−vis spectra for CeO_2, TA-CeO_2, Pt/CeO_2, and Pt/TA-CeO_2. (c) Plots of $(\alpha h\nu)^2$ vs photon energy ($h\nu$) for the Pt/CeO_2 and Pt/TA-CeO_2 catalysts. (d) H_2-TPR results of Pt/CeO_2 and Pt/TA-CeO_2.

(TOF) on the basis of the specific reaction rate and Pt content at 150 °C was calculated, and the TOF of Pt/TA-CeO_2 (0.075 s^{-1}) was approximately 2.5 times that of Pt/CeO_2 (0.030 s^{-1}), confirming the excellent catalytic activity of Pt/TA-CeO_2 for CO oxidation. The lower apparent activation energy (E_a) of Pt/TA-CeO_2 (51.8 ± 0.2 kJ·mol^{-1}) compared to that of Pt/CeO_2 (74.9 ± 0.3 kJ·mol^{-1}) corroborated the viewpoint that TA modification was beneficial for the activation of reactants on the Pt/TA-CeO_2 catalyst (Figure 1c). Furthermore, the reaction orders of CO and O_2 over Pt/TA-CeO_2 (0.44 ± 0.03 and 0.42 ± 0.01, respectively) were both lower than those over Pt/CeO_2 (0.55 ± 0.04 and 0.47 ± 0.03, respectively), as shown in Figure 1d, which indicated that robust Pt sites for the adsorption and activation of CO and O_2 were constructed on Pt/TA-CeO_2.[25−27] Generally, TA modification might have significantly altered Pt dispersion and the interplay between Pt and CeO_2, which could be the main reason for the improved activity of Pt/TA-CeO_2 for CO oxidation. Thus, it was of great value to probe the structure−performance relationship of Pt/TA-CeO_2 and Pt/CeO_2 for CO oxidation.

3.2. Structural Characterization. According to the results of inductively coupled plasma optical emission spectrometer (ICP-OES) analysis, Pt/CeO_2 (0.63 wt %) and Pt/TA-CeO_2 (0.55 wt %) showed comparable Pt loadings (Table S2). To probe the structures of Pt/CeO_2 and Pt/TA-CeO_2, powder X-ray diffraction (XRD) patterns were first collected and shown in Figure 2a. It was obvious that all peaks in the XRD patterns for Pt/CeO_2 and Pt/TA-CeO_2 were associated with CeO_2 with a cubic fluorite structure (JCPDS 34-0394), and no peaks assigned to Pt^0/PtO_x emerged, suggesting that Pt species on CeO_2 and TA-CeO_2 were highly dispersed. EDS mapping images (Figure S5) showed that the distribution of N followed well with that of Ce and O, suggesting homogeneous doping of N. The absence of S on Pt/TA-CeO_2 indicated that thiourea decomposed during the hydrothermal treatment process, and residual N was doped into the lattice of CeO_2 (Table S3). Furthermore, as shown in the XPS spectrum of N 1s (Figure S6), the peak located at ca. 339.5 eV suggested that N atoms were in the form of N^{3-} instead of nitrates/nitrites.[28,29] Besides, in order to balance the surface charge, N^{3-} must have partially substituted the O^{2-} species bonded to $Ce^{3+/4+}$. That is, N−Ce−O structures were formed in Pt/TA-CeO_2,[30−33] further confirming that N anions were incorporated successfully into the crystal lattice of CeO_2. Moreover, all the peaks for Pt/TA-CeO_2 shifted to higher angles (ca. 0.06° higher than those for Pt/CeO_2, Figure 2b), and the unit cell parameter of Pt/TA-CeO_2 (5.394 Å) was smaller than that of Pt/CeO_2 (5.399 Å), which revealed lattice contraction of CeO_2 resulted from the substitution of lattice O^{2-} by N anions.[34]

Thermogravimetric (TG) analysis was used to investigate the loss of N element in Pt/TA-CeO_2 in an air atmosphere (Figure S7). The TGA results show that there was no obvious difference between Pt/TA-CeO_2 and Pt/CeO_2 below 425 °C. When the temperature continued to increase, a significant weight loss (0.95%) occurred in Pt/TA-CeO_2, resulting from the loss of N-doped Pt/TA-CeO_2. Therefore, the loss of N under oxidized conditions was almost negligible during the CO oxidation reaction (below 200 °C). As confirmed by the TEM

https://doi.org/10.1021/acs.iecr.4c04820
Ind. Eng. Chem. Res. 2025, 64, 4835−4844

Table 1. Data Summary from the Raman Spectra and XPS Results

	parameters of Raman spectra	surface atomic concentration (%)					
samples	$I_{Pt-O-Ce+Pt-O}/I_{F2g}$	O	Ce	N	Pt	Ce^{3+}/total Ce (%)	Pt^{2+}/total Pt (%)
CeO_2		81.3	18.7			12.9	
TA-CeO_2		78.7	17.6	3.7		12.7	
Pt/CeO_2	0.32	83.5	15.4		1.1	17.3	89.8
Pt/TA-CeO_2	0.20	80.0	16.6	2.4	1.0	13.2	86.8

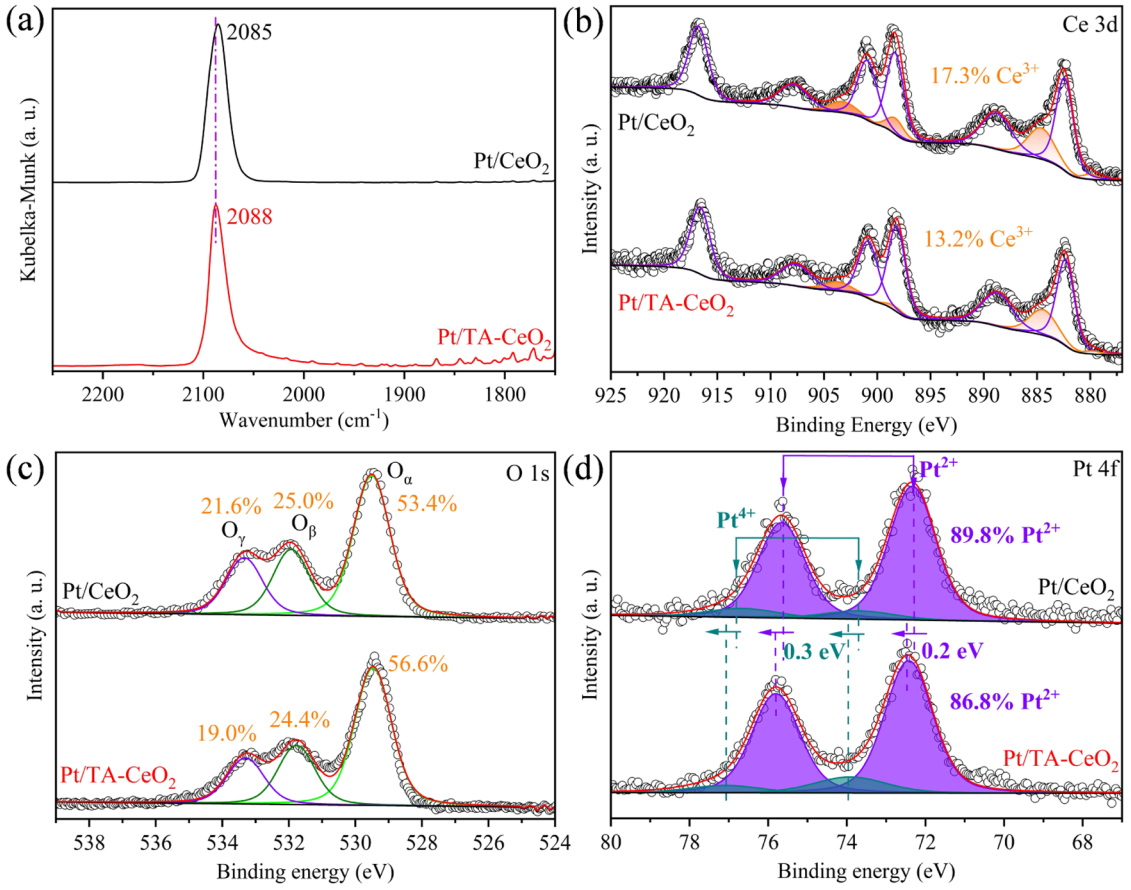

Figure 4. Electronic states of Pt and surface chemical states. (a) *In situ* CO-DRIFTS of Pt/CeO_2 and Pt/TA-CeO_2 catalysts before the CO oxidation reaction. (b) Ce 3d, (c) O 1s, and (d) Pt 4f XPS for Pt/CeO_2 and Pt/TA-CeO_2.

images, the two catalysts exhibited similar nanocube morphologies, and no Pt particles were observed (Figure 2c,2d). The isotherms of N_2 adsorption−desorption for Pt/CeO_2 and Pt/TA-CeO_2 were similar, exhibiting type IV isotherms with H3 hysteresis loops, and the BET surface areas of Pt/CeO_2 (17.5 $m^2 \cdot g^{-1}$) and Pt/TA-CeO_2 (16.8 $m^2 \cdot g^{-1}$) were almost the same, which meant that the surface area and pore structure were not the key factors accounting for their different catalytic performances (Figure S8 and Table S2).

To further investigate the structure of all catalysts, Raman spectra were collected and are presented in Figure 3a. For pure CeO_2 and TA-CeO_2, two peaks at ca. 464 and 590 cm^{-1} could be attributed to the F_{2g} mode of Ce−O vibration in the fluorite-type CeO_2 lattice and the defect-induced mode because of the presence of oxygen vacancies in CeO_2.[17,35] After Pt loading, the band related to the F_{2g} mode shifted to lower wavenumbers (464 → 450 cm^{-1}), and the half-width of F_{2g} increased, which could originate from the strong interaction between Pt and CeO_2. Moreover, the two new peaks at ca. 557 and 648 cm^{-1} were observed on Pt/CeO_2 and Pt/TA-CeO_2, which were attributed to the vibrations of Pt−O−Ce and Pt−O (in Pt−O−Ce) configurations, respectively.[36] The relative concentration of the Pt−O−Ce structure could be represented as the peak area ratio of the Pt−O−Ce/Pt−O peaks to the CeO_2 F_{2g} peak, i.e., $I_{Pt-O-Ce+Pt-O}/I_{F2g}$. The relative concentration of the Pt−O−Ce structure on Pt/TA-CeO_2 (0.20) was lower than that on Pt/CeO_2 (0.32) (Table 1), indicating that the doping of N into CeO_2 could have weakened the interplay between the Pt species and CeO_2 support.[37]

The UV−vis spectra for CeO_2, TA-CeO_2, Pt/CeO_2, and Pt/TA-CeO_2 were also collected to further explore the physicochemical properties. All catalysts presented a characteristic absorption region related to CeO_2 below 400 nm (Figure 3b). In detail, the band at around 266 nm was assigned to charge transfer from O_{2p} to Ce_{4f}, and the band at about 338 nm was attributed to interband transitions.[38] Upon Pt deposition, a new absorption band associated with the absorption or Urbach tail that was caused by the band gap smearing emerged in the range of 400−600 nm,[14] which was

https://doi.org/10.1021/acs.iecr.4c04820
Ind. Eng. Chem. Res. 2025, 64, 4835−4844

associated with the structural distortion and surface defects induced by the highly dispersed Pt species.[39] Moreover, the adsorption intensity for Pt/TA-CeO_2 decreased by 35% compared to Pt/CeO_2, suggesting that fewer surface defects were formed on Pt/TA-CeO_2, possibly due to the weaker interactions between Pt atoms and the CeO_2 support.[14] The direct band gap for the catalysts was further estimated using the Davis and Mott equation to probe the interplay between Pt atoms and CeO_2 support (Figures S9 and 3c).[40] The band gap for CeO_2 (3.14 eV) and TA-CeO_2 (3.13 eV) were comparable (Figure S9), while it decreased after Pt loading, indicating that the formation of Pt-CeO_2 interaction could influence the electronic structure of CeO_2.[41] Moreover, the band gap for Pt/TA-CeO_2 (3.00 eV) was larger than that of Pt/CeO_2 (2.85 eV) (Figure 3c), indicating that the Pt−O−Ce interaction in Pt/TA-CeO_2 was weaker than that in Pt/CeO_2, consistent with the results of Raman spectra.

H_2-TPR experiments were employed to evaluate the redox properties of the catalysts as well as the strength of the Pt−O−Ce interaction in the Pt/CeO_2 catalysts.[42] As shown in Figure 3d, three H_2-consumption peaks (α, β, and γ) emerged for Pt/CeO_2 and Pt/TA-CeO_2 from 50 to 450 °C, which could be attributed to the reduction of the Pt−O/Pt−O-Ce structure (100 °C), CeO_2 adjacent to Pt species (150−220 °C), and surface Ce^{4+} (300−450 °C), respectively.[17,43,44] Notably, after thiourea modification, the position of the H_2-consumption peaks ascribed to the reduction of the Pt−O/Pt−O-Ce structure and CeO_2 adjacent to Pt on Pt/CeO_2 shifted from 111 to 101 and 209 to 174 °C, respectively, further validating the Raman spectra and UV−vis results that the Pt−CeO_2 interaction in Pt/CeO_2 was weakened by thiourea modification. Notably, the relatively lower reduction temperature of the Pt−O−Ce/Pt−O structure on Pt/TA-CeO_2 suggested that Pt/TA-CeO_2 showed better redox performance than Pt/CeO_2.

3.3. Pt Dispersion and Surface Chemical States. It has been widely reported that the dispersion of Pt species could significantly determine their catalytic performance.[7,45] To elucidate the dispersion of Pt species on Pt/CeO_2 and Pt/TA-CeO_2 before and after the CO oxidation reaction, *in situ* diffuse reflectance infrared Fourier transform spectroscopy of the CO adsorption (CO-DRIFTS) experiment was performed. As shown in Figure 4a, for fresh catalysts, only one intensive IR band associated with linearly adsorbed CO on the ionic Pt sites (CO@$Pt^{\delta+}$) was captured on Pt/TA-CeO_2 and Pt/CeO_2 within the range of 1750−2250 cm^{-1},[46] indicating that Pt SACs were successfully constructed on both Pt/CeO_2 and Pt/TA-CeO_2. Moreover, the blue shift of the CO-IR band from 2085 to 2088 cm^{-1} after thiourea modification indicated that the doping of N into ceria could change the electronic state of the Pt atoms.

The dispersion of the Pt species after the CO oxidation activity test was also investigated through *in situ* CO-DRIFTS (Figure S10). After the treatment by CO oxidation reaction flow, in addition to the CO@$Pt^{\delta+}$ band, a CO band at ca. 2120 cm^{-1} was also captured on Pt/CeO_2 and Pt/TA-CeO_2, which could be attributed to CO adsorbed on $Pt^{\delta+}$ with higher oxidation states.[47] It should be noted that the new emerging band (located at ca. 2120 cm^{-1}) on Pt/CeO_2 (74.4%) was much more intensive than that on Pt/TA-CeO_2 (3.1%) (Figure S11), and the CO@$Pt^{\delta+}$ band on Pt/CeO_2 also shifted from 2085 to 2089 cm^{-1}, suggesting that Pt SACs anchored on TA-CeO_2 were much more stable than those on CeO_2, which should be related to the N doping effect on Pt/TA-CeO_2. Moreover, according to the results of the CO-DRIFTS experiment on Pt/CeO_2 and Pt/TA-CeO_2 catalysts after the long-term CO oxidation test (Figure S12), an intensive CO-IR band at ca. 2068 cm^{-1}, attributed to CO adsorbed on aggregated Pt clusters/particles, was observed on Pt/CeO_2,[48] indicating that Pt single atoms on Pt/CeO_2 aggregated to clusters/particles after the 6 h test. In clear contrast, for used Pt/TA-CeO_2, the presence of intensive bands at ca. 2084 cm^{-1} related to CO adsorbed on Pt single atoms and the absence of an exclusive CO-IR band attributed to CO adsorbed on Pt clusters/particles suggested that Pt species on Pt/TA-CeO_2 were still mainly in the form of single atoms. In short, the Pt single atoms on Pt/TA-CeO_2 exhibited better stability than those on Pt/CeO_2. The ability of Pt/TA-CeO_2 to maintain the supported Pt ions in relatively lower valence and avoid its further agglomeration into clusters should be the key reason for its superior activity and stability for CO oxidation.[49]

To better elucidate the surface states of all catalysts, an XPS experiment was conducted, and the results are shown in Figures 4b−d, S13 and Table 1. For Ce 3d XPS (Figures 4b and S13a), the surface Ce^{3+} concentrations (i.e., $Ce^{3+}/(Ce^{3+} + Ce^{4+})$) of CeO_2 (12.9%) and TA-CeO_2 (12.7%) were comparable. After loading Pt, the concentration of Ce^{3+} on CeO_2 and TA-CeO_2 increased to 17.3% and 13.2%, respectively. Considering that Ce^{3+} within CeO_2 is usually accompanied by the presence of oxygen vacancies, a higher concentration of Ce^{3+} species in Pt/CeO_2 indicates the presence of more oxygen vacancies, which should be related to the stronger metal−support interaction in Pt/CeO_2 compared with that in Pt/TA-CeO_2.[50] O 1s XPS were also acquired (Figures 4c and S13b). Three peaks located at 529.5, 531.8, and 533.3 eV were attributed to lattice oxygen species (O_α), oxygen vacancy-related oxygen species (O_β), and chemisorbed oxygen species closely related to the adsorbed hydroxyl groups on the surface (O_γ), respectively.[51] Although the relative concentrations of surface oxygen species $((O_\beta + O_\gamma)/(O_\alpha + O_\beta + O_\gamma))$ on CeO_2 (32.3%) and TA-CeO_2 (32.9%) were almost the same, Pt/CeO_2 (46.6%) possessed more surface oxygen species than Pt/TA-CeO_2 (43.4%), matching well with the result of Ce 3d XPS since the generation of Ce^{3+} was always accompanied by more surface oxygen vacancies and adsorbed oxygen species.[46] To determine the influence of N doping on the electronic state of Pt species, Pt 4f XPS data were also collected (Figure 4d). In the case of Pt/CeO_2, there were two predominant peaks centered at 72.3 and 75.6 eV ascribed to Pt^{2+} species, and two peaks centered at 73.7 and 76.8 eV associated with the Pt^{4+} species, indicating that the Pt species on Pt/CeO_2 mainly existed as Pt^{2+}. For Pt/TA-CeO_2, the Pt 4f XPS peaks shifted to higher binding energies (72.5 and 75.8 eV for Pt^{2+}, 74.0 and 77.1 eV for Pt^{4+}), indicating that the average oxidation state of Pt species on Pt/CeO_2 was slightly higher than those on Pt/TA-CeO_2.

XPS valence band photoemission spectra for CeO_2 before and after Pt deposition were collected and are plotted in Figure S14, which were used to detect the peak position of the Pt species. The valence band spectrum for the pristine CeO_2 support exhibited a significant band gap associated with the Ce_{4f}−O_{2p} band within the range of 2.5−7.5 eV.[52] Upon Pt deposition, a new feature peak emerged at around 1.4 eV, which originated from Pt 5d states.[52] Meanwhile, it is noteworthy that the density of states (DOS) near the Fermi level (E_F) for Pt/CeO_2 approached zero (Figure S14). Since

https://doi.org/10.1021/acs.iecr.4c04820
Ind. Eng. Chem. Res. 2025, 64, 4835−4844

the valence band spectrum of bulk platinum could be observed at the Fermi level with a notably high DOS,[53] it could be proposed that no metallic platinum species were formed on the Pt/CeO_2 catalyst. Previously, Nørskov et al. proposed a band model based on DFT calculations to elucidate the impact of the d-band center on the surface adsorption energy, a critical parameter reflecting the adsorption capability of the catalyst surface.[54] According to their work, to identify the adsorption capability of $Pt/TA\text{-}CeO_2$ and Pt/CeO_2, d-band centers of Pt 5d states were calculated according to the XPS valence band results (Figure S15). The d-band centers of Pt/CeO_2 and $Pt/TA\text{-}CeO_2$ were −1.26 and −1.15 eV, respectively. Obviously, the d-band center of $Pt/TA\text{-}CeO_2$ moved closer to the Fermi level than that of Pt/CeO_2, revealing that the adsorption capability of $Pt/TA\text{-}CeO_2$ for the reactants was enhanced after N doping.

3.4. Discussion. As discussed above, the detailed structures of Pt/CeO_2 and $Pt/TA\text{-}CeO_2$ are proposed. Specifically, the results of CO-DRIFTS, XPS, and valence band spectroscopy indicated that the Pt species in Pt/CeO_2 and $Pt/TA\text{-}CeO_2$ were in the form of isolated $Pt^{\delta+}$. Moreover, the Raman spectra and H_2-TPR results further revealed that thiourea modification would inhibit the formation of Pt−O−Ce linkages and weaken the $Pt\text{−}CeO_2$ interaction on Pt/CeO_2. Besides, the absence of S element and the presence of N element with negative valence on $Pt/TA\text{-}CeO_2$ suggested that the addition of thiourea during the hydrothermal treatment process when preparing the $TA\text{-}CeO_2$ support results in the formation of N-doped CeO_2, in which the lattice O^{2-} of CeO_2 was partially substituted by N anions. Therefore, it could be deduced that N doping could be the most critical reason for the lower Pt−O−Ce concentration and weaker $Pt\text{−}CeO_2$ interaction in $Pt/TA\text{-}CeO_2$ than in Pt/CeO_2. Herein, a concise surface model of Pt/CeO_2 and $Pt/TA\text{-}CeO_2$ is proposed (Figure 5). As reported previously, the

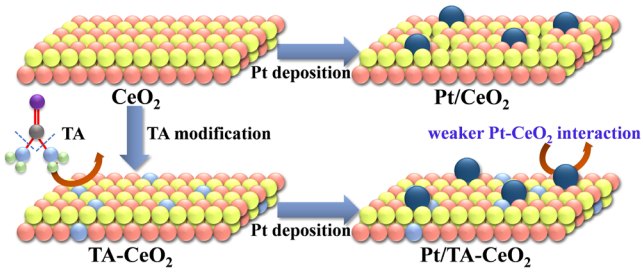

Figure 5. Schematic representation of the surface model of Pt/CeO_2 and $Pt/TA\text{-}CeO_2$. Dark blue: Pt, yellow: Ce, red: O, light blue: N, purple: S, green: H, and gray: C.

reaction between adsorbed CO on Pt single atoms and the O within the Pt−O−Ce structure was one of the rate-determining steps for CO oxidation on Pt/CeO_2 catalysts.[14] In this work, as confirmed by H_2-TPR, the oxygen atoms within the Pt−O/Pt−O-Ce structure in $Pt/TA\text{-}CeO_2$ with weaker $Pt\text{−}CeO_2$ interaction showed a better low-temperature reactivity than those on Pt/CeO_2, which could be the key reason for the better activity of $Pt/TA\text{-}CeO_2$ for CO oxidation.

4. CONCLUSIONS

In this work, a novel strategy for the modulation of the $Pt\text{−}CeO_2$ interaction strength on CeO_2-supported Pt SACs was proposed. It was found that the substitution of lattice O^{2-} in CeO_2 by N anions, which were introduced by adding thiourea during the hydrothermal synthesis of the CeO_2 support, could inhibit the formation of Pt−O−Ce, weaken the $Pt\text{−}CeO_2$ interaction, and tune the electronic states of the Pt sites. As a result, the improved reactivity of O within the Pt−O/Pt−O-Ce structure was achieved on $Pt/TA\text{-}CeO_2$, thus generating better low-temperature CO oxidation activity. This work can provide valuable insight into the manipulation of metal−support interactions on supported catalysts for industrially important catalytic reactions.

■ ASSOCIATED CONTENT

Data Availability Statement

Data will be made available on request.

Supporting Information

The Supporting Information is available free of charge at https://pubs.acs.org/doi/10.1021/acs.iecr.4c04820.

Experimental procedures, SEM images, EDS mapping, XPS data, N_2 adsorption isotherms, TG analysis, *in situ* CO-DRIFTS, and comparison data (PDF)

■ AUTHOR INFORMATION

Corresponding Authors

Wei Tan − *State Key Laboratory of Pollution Control and Resource Reuse, School of Environment, Jiangsu Key Laboratory of Vehicle Emissions Control, Center of Modern Analysis, Key Laboratory of Mesoscopic Chemistry of MOE, School of Chemistry and Chemical Engineering, Nanjing University, Nanjing, Jiangsu 210023, China;* orcid.org/0000-0002-1481-9346; Email: tanwei@nju.edu.cn

Yang Lou − *Key Laboratory of Synthetic and Biological Colloids, Ministry of Education, School of Chemical and Material Engineering, Jiangnan University, Wuxi, Jiangsu 214122, China; International Joint Research Center for Photoresponsive Molecules and Materials, Jiangnan University, Wuxi, Jiangsu 214122, China;* orcid.org/0000-0002-8310-8150; Email: yang.lou@jiangnan.edu.cn

Authors

Lijun Ni − *Key Laboratory of Synthetic and Biological Colloids, Ministry of Education, School of Chemical and Material Engineering, Jiangnan University, Wuxi, Jiangsu 214122, China; International Joint Research Center for Photoresponsive Molecules and Materials, Jiangnan University, Wuxi, Jiangsu 214122, China*

Bifeng Zhang − *State Key Laboratory of Pollution Control and Resource Reuse, School of Environment, Jiangsu Key Laboratory of Vehicle Emissions Control, Center of Modern Analysis, Key Laboratory of Mesoscopic Chemistry of MOE, School of Chemistry and Chemical Engineering, Nanjing University, Nanjing, Jiangsu 210023, China*

Qi Zhang − *Key Laboratory of Synthetic and Biological Colloids, Ministry of Education, School of Chemical and Material Engineering, Jiangnan University, Wuxi, Jiangsu 214122, China; International Joint Research Center for Photoresponsive Molecules and Materials, Jiangnan University, Wuxi, Jiangsu 214122, China*

Jing Xu − *School of Food Science and Technology, Jiangnan University, Wuxi, Jiangsu 214122, China*

Ying Zhang − *Key Laboratory of Synthetic and Biological Colloids, Ministry of Education, School of Chemical and Material Engineering, Jiangnan University, Wuxi, Jiangsu 214122, China; International Joint Research Center for*

https://doi.org/10.1021/acs.iecr.4c04820
Ind. Eng. Chem. Res. 2025, 64, 4835−4844

Photoresponsive Molecules and Materials, Jiangnan University, Wuxi, Jiangsu 214122, China

Chengsi Pan − *Key Laboratory of Synthetic and Biological Colloids, Ministry of Education, School of Chemical and Material Engineering, Jiangnan University, Wuxi, Jiangsu 214122, China; International Joint Research Center for Photoresponsive Molecules and Materials, Jiangnan University, Wuxi, Jiangsu 214122, China;* orcid.org/0000-0002-1624-4259

Yongfa Zhu − *Department of Chemistry, Tsinghua University, Beijing 100084, China;* orcid.org/0000-0001-8528-509X

Fudong Liu − *Department of Chemical and Environmental Engineering, University of California, Riverside, California 92521, United States;* orcid.org/0000-0001-8771-5938

Complete contact information is available at: https://pubs.acs.org/10.1021/acs.iecr.4c04820

Author Contributions

L.N.: data curation, formal analysis, writing-original draft, review, and editing. W.T.: formal analysis, writing-original draft, review and editing. B.Z.: formal analysis. Q.Z.: data curation and formal analysis. J.X.: investigation. Y.Z.: data curation. C.P.: investigation. Y.Z.: methodology. F.L.: methodology. Y.L.: conceptualization, methodology, data curation, funding acquisition, writing-original draft, review, and editing.

Notes

The authors declare no competing financial interest.

■ ACKNOWLEDGMENTS

This project was supported financially by the National Key R&D Program of China (2021YFB3501900), National Natural Science Foundation of China (U21A20326, 22379054, and 22306090), Jiangsu Specially-Appointed Professor (1046010241211400), and Natural Science Foundation of Jiangsu Province (BK20211239, BK20230773). F.L. acknowledges the Startup Fund from the University of California, Riverside (UCR). The authors gratefully acknowledge the use of facilities within the Central Laboratory, School of Chemical and Material Engineering at Jiangnan University.

■ REFERENCES

(1) Jones, J.; Xiong, H. F.; Delariva, A. T.; Peterson, E. J.; Pham, H.; Challa, S. R.; Qi, G. S.; Oh, S.; Wiebenga, M. H.; Hernández, X. I. P.; Wang, Y.; Datye, A. K. Thermally stable single-atom platinum-on-ceria catalysts via atom trapping. *Science* **2016**, *353* (6295), 150−154.

(2) Chen, H.; Jie, K. C.; Jafta, C. J.; Yang, Z. Z.; Yao, S. Y.; Liu, M. M.; Zhang, Z. H.; Liu, J. X.; Chi, M. F.; Fu, J.; Dai, S. An ultrastable heterostructured oxide catalyst based on high-entropy materials: A new strategy toward catalyst stabilization via synergistic interfacial interaction. *Appl. Catal., B* **2020**, *276*, No. 119155.

(3) Grabchenko, M. V.; Mamontov, G. V.; Zaikovskii, V. I.; La Parola, V.; Liotta, L. F.; Vodyankina, O. V. The role of metal-support interaction in Ag/CeO_2 catalysts for CO and soot oxidation. *Appl. Catal., B* **2020**, *260*, No. 118148.

(4) Shi, Y.; Gu, Q.; Zhao, Y.; Ren, Y.; Yang, B.; Xu, J.; Zhang, Y.; Pan, C.; Zhu, Y.; Lou, Y. Local In-O-Pd Lewis acid-base pair boosting CO_2 selective hydrogenation to methanol. *Chem. Eng. J.* **2024**, *485*, No. 150093.

(5) Yu, Y.; Lin, G.; Song, W.; Wang, J.; Chen, H.; Fu, J.; Lou, Y. Strong Cu/ZnO interfacial interaction induced by ZrO_2 promoter suppressing the ethanol formation inindustrial methanol synthesis. *Ind. Eng. Chem. Res.* **2024**, *63* (28), 12459−12467.

(6) Yu, B.; Cheng, L.; Wu, J.; Yang, B.; Li, H.; Xu, J.; Zhang, Y.; Pan, C.; Cao, X.-M.; Zhu, Y.; Lou, Y. Surface hydroxyl group dominating aerobic oxidation of methane below room temperature. *Energy Environ. Sci.* **2024**, *17*, 8127−8139.

(7) Jiang, D.; Yao, Y.; Li, T. Y.; Wan, G.; Pereira-Hernández, X. I.; Lu, Y. B.; Tian, J. S.; Khivantsev, K.; Engelhard, M. H.; Sun, C. J.; Vargas, C. E. G.; Hoffman, A. S.; Bare, S. R.; Datye, A. K.; Hu, L.; Wang, Y. Tailoring the local environment of platinum in single-atom Pt_1/CeO_2 catalysts for robust low-temperature CO oxidation. *Angew. Chem., Int. Ed.* **2021**, *60* (50), 26054−26062.

(8) Xu, J.; Wang, Y.; Wang, K.; Zhao, M.; Zhang, R.; Cui, W. J.; Liu, L.; Bootharaju, M. S.; Kim, J. H.; Hyeon, T.; Zhang, H.; Wang, Y.; Song, S.; Wang, X. Single-atom Rh on high-index CeO_2 facet for highly enhanced catalytic CO oxidation. *Angew. Chem., Int. Ed.* **2023**, *62* (28), No. e202302877.

(9) Hou, Z. Q.; Lu, Y.; Liu, Y. X.; Liu, N.; Hu, J. C.; Wei, L.; Li, Z. Y.; Tian, X. R.; Gao, R. Y.; Yu, X. H.; Feng, Y.; Wu, L.; Deng, J.; Wang, D.; Sui, M.; Dai, H.; Li, Y. A general dual-metal nanocrystal dissociation strategy to generate robust high-temperature-stable alumina-supported single-atom catalysts. *J. Am. Chem. Soc.* **2023**, *145* (29), 15869−15878.

(10) Li, P.; Chen, X. Y.; Li, Y. D.; Schwank, J. W. A review on oxygen storage capacity of CeO_2-based materials: Influence factors, measurement techniques, and applications in reactions related to catalytic automotive emissions control. *Catal. Today* **2019**, *327*, 90−115.

(11) Kunwar, D.; Zhou, S. L.; DeLaRiva, A.; Peterson, E. J.; Xiong, H. F.; Pereira-Hernández, X. I.; Purdy, S. C.; ter Veen, R.; Brongersma, H. H.; Miller, J. T.; Hashiguchi, H.; Kovarik, L.; Lin, S.; Guo, H.; Wang, Y.; Daty, A. K. Stabilizing high metal loadings of thermally stable platinum single atoms on an industrial catalyst support. *ACS Catal.* **2019**, *9* (5), 3978−3990.

(12) Lou, Y.; Xu, J.; Zhang, Y.; Pan, C.; Dong, Y.; Zhu, Y. Metal-support interaction for heterogeneous catalysis: from nanoparticles to single atoms. *Mater. Today Nano* **2020**, *12*, No. 100093.

(13) Jin, S. Q.; Zhang, Z. K.; Li, D. D.; Wang, Y. M.; Lian, C.; Zhu, M. H. Alcohol-induced strong metal-support interactions in a supported copper/ZnO catalyst. *Angew. Chem. Int. Ed.* **2023**, *62*, No. e202301563.

(14) Tan, W.; Xie, S. H.; Le, D.; Diao, W. J.; Wang, M. Y.; Low, K. B.; Austin, D.; Hong, S. Y.; Gao, F.; Dong, L.; Ma, L.; Ehrlich, S. N.; Rahman, T. S.; Liu, F. Fine-tuned local coordination environment of Pt single atoms on ceria controls catalytic reactivity. *Nat. Commun.* **2022**, *13* (1), No. 7070.

(15) Ma, X.; Liu, H.; Yang, W. J.; Mao, G. Y.; Zheng, L. R.; Jiang, H. L. Modulating coordination environment of single-atom catalysts and their proximity to photosensitive units for boosting MOF photocatalysis. *J. Am. Chem. Soc.* **2021**, *143* (31), 12220−12229.

(16) Tan, W.; Xie, S. H.; Wang, X.; Wang, C. Y.; Li, Y. B.; Shaw, T. E.; Ma, L.; Ehrlich, S. N.; Liu, A. N.; Ji, J. W.; Gao, F.; Dong, L.; Liu, F. Highly efficient Pt catalyst on newly designed CeO_2-ZrO_2-Al_2O_3 support for catalytic removal of pollutants from vehicle exhaust. *Chem. Eng. J.* **2021**, *426*, No. 131855.

(17) Tan, W.; Xie, S. H.; Cai, Y. D.; Yu, H. W.; Ye, K. L.; Wang, M. Y.; Diao, W. J.; Ma, L.; Ehrlich, S. N.; Gao, F.; Dong, L.; Liu, F. Surface lattice-embedded Pt single-atom catalyst on ceria-zirconia with superior catalytic performance for propane oxidation. *Environ. Sci. Technol.* **2023**, *57* (33), 12501−12512.

(18) Yoon, S.; Ha, H.; Kim, J.; Nam, E.; Yoo, M.; Jeong, B.; Kim, H. Y.; An, K. Influence of the Pt size and CeO_2 morphology at the Pt-CeO_2 interface in CO oxidation. *J. Mater. Chem. A* **2021**, *9* (46), 26381−26390.

(19) Zhan, W. C.; He, Q.; Liu, X. F.; Guo, Y. L.; Wang, Y. Q.; Wang, L.; Guo, Y.; Borisevich, A. Y.; Zhang, J. S.; Lu, G. Z.; Dai, S. A sacrificial coating strategy toward enhancement of metal-support interaction for ultrastable Au nanocatalysts. *J. Am. Chem. Soc.* **2016**, *138* (49), 16130−16139.

(20) Chu, Y. Y.; Cao, J.; Dai, Z.; Tan, X. Y. A novel Pt/CeO_2 catalyst coated with nitrogen-doped carbon with excellent performance for DMFCs. *J. Mater. Chem. A* **2014**, *2* (11), 4038−4044.
(21) Liu, Y. M.; Xu, Q.; Fan, X. F.; Quan, X.; Su, Y.; Chen, S.; Yu, H. T.; Cai, Z. J. Electrochemical reduction of N_2 to ammonia on Co single atom embedded N-doped porous carbon under ambient conditions. *J. Mater. Chem. A* **2019**, *7* (46), 26358−26363.
(22) Pastor-Pérez, L.; Ramos-Fernández, E. V.; Sepúlveda-Escribano, A. Effect of the CeO_2 synthesis method on the behaviour of Pt/CeO_2 catalysis for the water-gas shift reaction. *Int. J. Hydrogen Energy* **2019**, *44* (39), 21837−21846.
(23) Yu, J.; Chen, W.; He, F.; Song, W.; Cao, C. Electronic oxide-support strong interactions in the graphdiyne-supported cuprous oxide nanocluster catalyst. *J. Am. Chem. Soc.* **2023**, *145* (3), 1803−1810.
(24) Wang, W.; Xiong, Z. B.; He, W. F.; Lu, W.; Shi, H. C. Influence of thiourea modification on the NH_3-SCR activity of CeO_2: Simultaneous tuning morphology and surface acidity. *J. Energy Inst.* **2021**, *98*, 322−333.
(25) Ni, L.; Zhou, Y.; Tan, W.; Li, H.; Wang, D.; Zhang, Q.; Yang, B.; Xu, J.; Zhang, Y.; Pan, C.; Zhu, Y.; Liu, F.; Lou, Y. Asymmetric coordinative modulation boosting the activity and thermal stability of Pt_1/CeO_2 for CO oxidation under harsh condition. *Chem. Eng. J.* **2024**, *501*, No. 157250.
(26) Zhao, Y.; Sun, X.; Gu, Q.; Wang, D.; Yang, B.; Xu, J.; Zhang, Y.; Pan, C.; Zhu, Y.; Lou, Y. Edge-confined Rh_2/MoS_2 dual-atom catalyst for selective activation of nitro group to amino group at room temperature. *Ind. Eng. Chem. Res.* **2024**, *63* (39), 16762−16769.
(27) Zhao, Y.; Gu, Q.; Sun, X.; Wang, D.; Gong, X.; Yang, B.; Xu, J.; Peng, B.; Zhang, Y.; Pan, C.; Zhu, Y.; Lou, Y. Steric-confinement Rh_2/MoS_2 dual-atom catalyst directionally modulating adsorption configuration of ester group to boost ethanol synthesis. *Chem* **2024**, *10*, 3342−3363.
(28) Gao, Y.; Fang, P.; Chen, F.; Liu, Y.; Liu, Z.; Wang, D.; Dai, Y. Enhancement of stability of N-doped TiO_2 photocatalysts with Ag loading. *Appl. Surf. Sci.* **2013**, *265*, 796−801.
(29) Dong, F.; Wang, H.; Wu, Z.; Qiu, J. Marked enhancement of photocatalytic activity and photochemical stability of N-doped TiO_2 nanocrystals by Fe^{3+}/Fe^{2+}. *J. Colloid Interface Sci.* **2010**, *343* (1), 200−208.
(30) Yan, X.; Gao, B.; Zheng, X.; Cheng, M.; Zhou, N.; Liu, X.; Du, L.; Yuan, F.; Wang, J.; Cui, X.; Zhang, G.; Kong, W.; Xu, Q. Cooperatively tailored surface frustrated Lewis pairs and N-doping on CeO_2 for photocatalytic CO_2 reduction to high-value hydrocarbon products. *Appl. Catal., B* **2024**, *343*, No. 123484.
(31) Jia, Z.; Ning, S.; Tong, Y.; Chen, X.; Hu, H.; Liu, L.; Ye, J.; Wang, D. Selective photothermal reduction of CO_2 to CO over Ni-nanoparticle/N-doped CeO_2 nanocomposite catalysts. *ACS Appl. Nano Mater.* **2021**, *4* (10), 10485−10494.
(32) Dao, D. V.; Nguyen, T. T. D.; Kim, D.-S.; Yoon, J.-W.; Yu, Y.-T.; Lee, I.-H. Core and dopant effects toward hydrogen gas sensing activity using Pd@N-CeO_2 core-shell nanoflatforms. *J. Ind. Eng. Chem.* **2021**, *95*, 325−332.
(33) Wu, C. Solvothermal synthesis of N-doped CeO_2 microspheres with visible light-driven photocatalytic activity. *Mater. Lett.* **2015**, *139*, 382−384.
(34) Van Dao, D.; Jung, H. D.; Nguyen, T. T. D.; Ki, S.-W.; Son, H.; Bae, K.-B.; Le, T. D.; Cho, Y.-H.; Yang, J.-K.; Yu, Y.-T.; Back, S.; Lee, I.-H. Defect-rich N-doped CeO_2 supported by N-doped graphene as a metal-free plasmonic hydrogen evolution photocatalyst. *J. Mater. Chem. A* **2021**, *9* (16), 10217−10230.
(35) Loridant, S. Raman spectroscopy as a powerful tool to characterize ceria-based catalysts. *Catal. Today* **2021**, *373*, 98−111.
(36) Filtschew, A.; Hofmann, K.; Hess, C. Ceria and its defect structure: new insights from a combined spectroscopic approach. *J. Phys. Chem. C* **2016**, *120* (12), 6694−6703.
(37) Brogan, M. S.; Dines, T. J.; Cairns, J. A. Raman Spectroscopic Study of the Pt-CeO_2 Interaction in the Pt/Al_2O_3-CeO_2 Catalyst. *J. Chem. Soc., Faraday Trans.* **1994**, *90* (10), 1461−1466.
(38) Rao, K. N.; Bharali, P.; Thrimurthulu, G.; Reddy, B. M. Supported copper-ceria catalysts for low temperature CO oxidation. *Catal. Commun.* **2010**, *11* (10), 863−866.
(39) Bugrova, T. A.; Kharlamova, T. S.; Svetlichnyi, V. A.; Savel'eva, A. S.; Salaev, M. A.; Mamontov, G. V. Insights into formation of Pt species in Pt/CeO_2 catalysts: Effect of treatment conditions and metal-support interaction. *Catal. Today* **2021**, *375*, 36−47.
(40) Tiwari, S.; Rathore, G.; Patra, N.; Yadav, A. K.; Bhattacharya, D.; Jha, S. N.; Tseng, C. M.; Liu, S. W.; Biring, S.; Sen, S. Oxygen and cerium defects mediated changes in structural, optical and photo-luminescence properties of Ni substituted CeO_2. *J. Alloys Compd.* **2019**, *782*, 689−698.
(41) Deshpande, S.; Patil, S.; Kuchibhatla, S.; Seal, S. Size dependency variation in lattice parameter and valency states in nanocrystalline cerium oxide. *Appl. Phys. Lett.* **2005**, *87*, No. 133113.
(42) Gao, Y. X.; Wang, W. D.; Chang, S. J.; Huang, W. X. Morphology effect of CeO_2 support in the preparation, metal-support interaction, and catalytic performance of Pt/CeO_2 catalysts. *ChemCatChem* **2013**, *5* (12), 3610−3620.
(43) Tan, W.; Alsenani, H.; Xie, S. H.; Cai, Y. D.; Xu, P.; Liu, A. N.; Ji, J. W.; Gao, F.; Dong, L.; Chukwu, E.; Yang, M.; Liu, F. Tuning single-atom Pt_1-CeO_2 catalyst for efficient CO and C_3H_6 oxidation: Size effect of ceria on Pt structural evolution. *ChemNanoMat* **2020**, *6* (12), 1797−1805.
(44) Tan, W.; Xie, S. H.; Cai, Y. D.; Wang, M. Y.; Yu, S. H.; Low, K. B.; Li, Y. J.; Ma, L.; Ehrlich, S. N.; Gao, F.; Dong, L.; Liu, F. Transformation of highly stable Pt single sites on defect engineered ceria into robust Pt clusters for vehicle emission control. *Environ. Sci. Technol.* **2021**, *55* (18), 12607−12618.
(45) Gashnikova, D.; Maurer, F.; Sauter, E.; Bernart, S.; Jelic, J.; Dolcet, P.; Maliakkal, C. B.; Wang, Y.; Wöll, C.; Studt, F.; Kübel, C.; Casapu, M.; Grunwaldt, J. Highly active oxidation catalysts through confining Pd clusters on CeO_2 nano-islands. *Angew. Chem., Int. Ed.* **2024**, *63* (35), No. e202408511.
(46) Zhang, Z. H.; Tian, J. S.; Lu, Y. B.; Yang, S. Z.; Jiang, D.; Huang, W. X.; Li, Y. X.; Hong, J. Y.; Hoffman, A. S.; Bare, S. R.; Engelhard, M. H.; Datye, A. K.; Wang, Y. Memory-dictated dynamics of single-atom Pt on CeO_2 for CO oxidation. *Nat. Commun.* **2023**, *14*, No. 2664.
(47) Wang, M.; Zhang, Y.; Wu, Z.; Zheng, Y.; Zhou, Z.; Weng, W. Redox dynamics of platinum species on CeO_2 during CO oxidation reaction. *Chem. Eng. J.* **2022**, *450*, No. 138171.
(48) Zhang, Q.; Tang, X.; Zhou, Y.; Shi, Y.; Ni, L.; Xu, J.; Pan, C.; Zhang, Y.; Mu, B.; Guo, Y.; Lou, Y. Establishing metal-nonoxygen bonds to improve thermal stability of Pt_1/CeO_2 via coating boron nitride. *Chem. Eng. Sci.* **2025**, *302*, No. 120856.
(49) Derevyannikova, E. A.; Kardash, T. Y.; Stadnichenko, A. I.; Stonkus, O. A.; Slavinskaya, E. M.; Svetlichnyi, V. A.; Boronin, A. I. Structural insight into strong Pt-CeO_2 interaction: from single Pt atoms to PtO_x clusters. *J. Phys. Chem. C* **2019**, *123* (2), 1320−1334.
(50) Xu, H. D.; Zhang, Z. H.; Liu, J. X.; Do-Thanh, C. L.; Chen, H.; Xu, S. H.; Lin, Q. J.; Jiao, Y.; Wang, J. L.; Wang, Y.; Chen, Y.; Dai, S. Entropy-stabilized single-atom Pd catalysts via high-entropy fluorite oxide supports. *Nat. Commun.* **2020**, *11*, No. 3908.
(51) Yang, S.; Shen, H.; Cheng, F.; Wu, C.; Cao, Y.; Zhuo, S.; Zhang, Q.; Zhang, H. Organometallic precursor induced defect-enriched mesoporous CeO_2 with high specific surface area: preparation and catalytic performance. *J. Mater. Chem. A* **2020**, *8* (28), 14006−14014.
(52) Zhang, F.; Gutiérrez, R. A.; Lustemberg, P. G.; Liu, Z.; Rui, N.; Wu, T.; Ramírez, P. J.; Xu, W.; Idriss, H.; Ganduglia-Pirovano, M. V.; Senanayake, S. D.; Rodriguez, J. A. Metal-support interactions and C1 chemistry: transforming Pt-CeO_2 into a highly active and stable catalyst for the conversion of carbon dioxide and methane. *ACS Catal.* **2021**, *11* (3), 1613−1623.
(53) Wu, D.; Kusada, K.; Yamamoto, T.; Toriyama, T.; Matsumura, S.; Gueye, I.; Seo, O.; Kim, J.; Hiroi, S.; Sakata, O.; Kawaguchi, S.; Kubota, Y.; Kitagawa, H. On the electronic structure and hydrogen

https://doi.org/10.1021/acs.iecr.4c04820
Ind. Eng. Chem. Res. 2025, 64, 4835−4844

evolution reaction activity of platinum group metal-based high-entropy-alloy nanoparticles. *Chem. Sci.* **2020**, *11* (47), 12731−12736.
(54) Hammer, B.; Nørskov, J. K. Theoretical surface science and catalysis-calculations and concepts. *Adv. Catal.* **2000**, *45*, 71−129.

https://doi.org/10.1021/acs.iecr.4c04820
Ind. Eng. Chem. Res. 2025, 64, 4835−4844